The Effects of Rotation on Boundary Layers in Turbomachine Rotors[1]

JAMES P. JOHNSTON

Stanford University

The boundary layers in turbomachine rotors are subject to Coriolis forces which can (1) contribute directly to the development of secondary flows and (2) indirectly influence the behavior of boundary layers by augmentation and/or suppression of turbulence production in the boundary layers on blades. Both these rotation-induced phenomena are particularly important in the development of understanding of flow and loss mechanisms in centrifugal and mixed flow machines. The primary objective of this paper is to review the information available on these effects.

Prediction of the behavior of the fluid boundary layers in the rotors of a turbomachine is largely based on information derived from experience with stationary systems. Nevertheless, when viewed from stationary (inertial) coordinates, rotor flow is periodically unsteady, and when viewed from rotor attached (rotating) coordinates, although the relative flow is steady,[2] Coriolis and centrifugal accelerations must be included in the dynamic equations of motion (see Appendix I). No matter how one tries, dimensional analysis (see Appendix II) shows that a rotation parameter, in addition to the standard parameters—Mach number, Reynolds number, specific heat ratio, etc.—is required to fully specify gross flow conditions in a rotor. There is then no assurance that stationary flow results will provide an adequate basis for rotor flow analysis. Investigation of the important effects of rotation on boundary layers is the main theme of this paper.

---

[1] The present study was conducted under National Science Foundation Grant No. GK-2533.

[2] Unsteadiness due to pressure fields of adjacent stators and stationary blade wake effects are not considered in this paper.

The most appropriate rotation parameter depends on the particular application. The well-known Ekmann and Taylor numbers (see Appendix II) are sometimes useful, but in turbomachine applications we have found the rotation number, $Ro = 2\omega L/U$, which expresses, in a general way, the ratio of Coriolis to inertial forces in the relative flow, to be most useful. Ro is the inverse of the well-known Rossby number, $Ros = Ro^{-1}$, of geophysical applications. For example, in consideration of the general circulation of ocean basins or the earth's atmosphere an important characteristic is $Ros \ll 1$ and $Ro \gg 1$. However, for rotor flows, the opposite is generally the case, $Ros > 1$ and $Ro < 1$; that is, Coriolis accelerations in rotor boundary layers are generally small, but, as will become evident, not always unimportant.

Probably the most significant rotation number for a boundary layer is formed from δ, a boundary layer thickness, and a characteristic relative free-stream velocity, U_∞. In these terms Ro becomes, with the further insertion of rotor parameters,

$$Ro \triangleq \frac{2\omega\delta}{U_\infty} = 2\,\frac{u_{tip}}{U_\infty}\,\frac{\delta}{r_{tip}}$$

In most applications u_{tip}/U_∞ is limited to a range of magnitudes from 10 to 1. Thus, the maximum value of Ro is roughly

$$(Ro)_{max} \approx 20\,\frac{\delta}{r_{tip}}$$

In turbine rotors, boundary layers are very thin, $\delta/r_{tip} < 10^{-3}$. Hence $(Ro)_{max} < 10^{-2}$, and neglect of rotation effects is probably justified. At the other end of the spectrum are the layers in centrifugal compressors and pump impellers, where δ/r_{tip} may be as large as 10^{-1} and $(Ro)_{max} \lesssim 1$ indicating the relatively large influence of Coriolis forces. In most applications, values of $Ro \lesssim 10^{-1}$ are more common. However, it has already been pointed out by Dean (ref. 11) that one cannot hope to understand the fluid dynamics of centrifugal rotor flow without an understanding of the effects that arise from system rotation.

Rotation manifests its influence on rotor boundary layers primarily through its effects on (1) *secondary flow*, and (2) *stability*, in the broadest sense. Each effect is considered briefly in the context of a radial-flow compressor, or pump, impeller passage.

Figure 1 illustrates a typical impeller and shows some characteristic relative velocity profiles inside, but near, the impeller exit plane. Profiles of this type have been shown experimentally a number of times (refs. 20, 16, 14, 33, 15, and 25) and may be inferred from other experiments (refs. 13 and 1, for example). The real relative velocity profiles always appear to be grossly different from those expected on the basis of inviscid

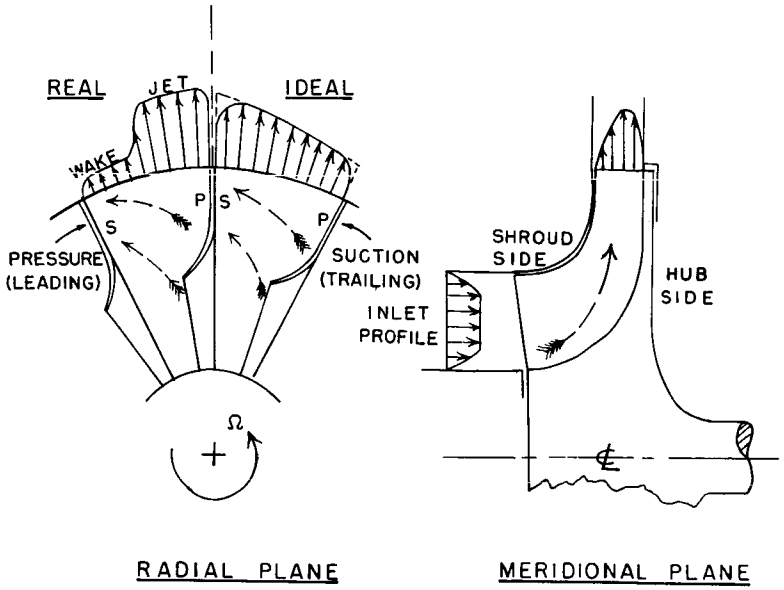

FIGURE 1.—*Centrifugal impeller flow. Dashed arrows indicate secondary flows.*

theory and normal boundary layer methods. It is common to find a thick wakelike region[3] near the blade trailing (suction) surface. This wake may result from more than one cause—certainly the deceleration of the trailing surface boundary layer contributes to the wake. However, secondary flows that arise from local layer growth and inlet total head deficits on the hub and shroud feed "tired" fluid into the trailing surface layer and thereby enhance the growth of the wake.

Secondary flow in the hub and shroud layers in the straight radial section of an impeller is a direct consequence of rotation. These low-speed layers are driven toward the trailing (suction) surface by the primary blade-to-blade tangential pressure field required to balance the Coriolis acceleration in the high-speed, relative, through flow. The qualitative aspects of secondary flows in centrifugal impellers are well illustrated in the visual studies of Senoo, et al. (ref. 42).

Although little work has been published to date on the effects of rotation on laminar boundary layer stability and the consequences of the stabilizing effects of rotation on turbulence, the idea that rotation can affect stability is not new; e.g., the classic study of G. I. Taylor (ref. 45) in 1932. Of more direct interest are the pioneering studies of Trefethen

[3] The consequences of the wake-jet effect on downstream flow and stage losses are discussed in references 11, 26, and 41.

(refs. 47 and 48) on laminar, transitional, and turbulent flow in long tubes that rotated about an axis perpendicular to the tube axis. In addition to noting the importance of secondary flows, he recognized that the transverse pressure gradients induced by Coriolis acceleration could affect the process of transition to turbulence by a mechanism similar to those operating in horizontal shear layers with density stratification.

The basic stabilizing mechanism is relatively easy to understand for a simple shear layer in a plane that rotates about an axis perpendicular to the plane of flow (fig. 2). A mean pressure gradient, $d\bar{p}^*/dy$, is required to balance the local mean Coriolis force, $2\rho\Omega\bar{u}$. Assume that a fluid particle is perturbed in the y direction to an adjacent layer (layer 1 to 2, fig. 2) while retaining its original mean velocity. The particle will be dynamically out of balance with the local mean pressure field at layer 2 and will tend to be accelerated away from its equilibrium layer, layer 1, if Ω is a positive number. In this crude sense, the flow is said to be destabilized by rotation. If Ω were negative, the particle would tend to return to its original position and the flow would be stabilized by rotation. From arguments of this type, one may derive a local profile stability parameter,

$$S=\frac{-2\Omega}{d\bar{u}/dy} \tag{1}$$

Positive values of S indicate stability and negative values instability. More exact reasoning, based on analogy to flows with mean streamline curvature[4] and horizontally stratified shear layers with vertical density gradients where centrifugal or buoyancy forces produce normal pressure gradients, led Bradshaw (ref. 7) to conclude that the proper local stability

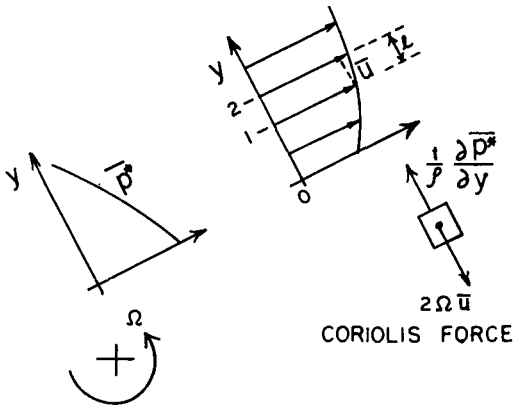

FIGURE 2.—*Pressure and velocity profiles in plane rotating shear flow.*

[4] See the classical inviscid stability analysis of Rayleigh (ref. 40) for curved flow.

parameter for plane rotating shear layers is the gradient Richardson number

$$Ri=\frac{-2\Omega[(d\bar{u}/dy)-2\Omega]}{(d\bar{u}/dy)^2}=S(1+S) \tag{2}$$

where $Ri>0$ indicates the tendency for rotation to stabilize, and $Ri<0$ to destabilize, the flow. The term

$$2\Omega-\frac{d\bar{u}}{dy}=\bar{\xi}_{abs} \tag{3}$$

is the absolute vorticity and should appear in a parameter of this type. Flow with zero absolute vorticity, whether rotating or stationary, should be neutrally stable to transverse perturbations (ref. 40). In conclusion, it must be recognized that this stability criterion takes no account of viscous effects which may increase, or decrease, the stability of the flow.

For our centrifugal impeller flow, figure 1, the trailing (suction) side boundary layers should be stabilized by rotation as $Ri>0$. Conversely, on the leading (pressure) side they should be less stable than in similar, but nonrotating, flows. If the main core of the flow is induced from an isothermal, stationary atmosphere, it will be irrotational, $\bar{\xi}_{abs}=0$, and neutrally stable even though $S<0$ in this region. In real flows, the shear layer separating the trailing side wake from the main flow (jet) should be more than normally stable because $Ri>0$ in this region.

The consequences of these stabilizing effects on centrifugal impeller flow are incompletely understood, but Dean (ref. 11) has elucidated them in part. In the stabilized, trailing side layer and the wake-jet shear layer, transition to turbulence may be inhibited and/or the normal turbulent mixing processes reduced in magnitude and effect. On the leading side the opposite effects can occur. The stabilized trailing side layer, under an adverse streamwise pressure gradient, may incur premature separation as a result of reduced turbulent stress levels. The reduction of mixing effectiveness in the wake-jet shear layer may contribute to the sometimes rather steep velocity gradients.

The computation of real flows in real centrifugal impellers is not possible today, in part due to lack of knowledge of the quantitative effects of rotational stabilization and in part due to the complex geometry of the blade passages. The basic theory of secondary flow in viscous boundary layers is known[5] for rotational flows as well as stationary flows, but the geometric complications (e.g., corners) and the interaction of the growing layers with the core flow, especially if stall occurs in a blade passage,

[5] The exception is turbulent layers in corners. Theory for three-dimensional thin turbulent layers on essentially flat walls is currently developing rapidly.

make direct application of theory problematical. Only for very simplified geometries and conditions has progress been made in the quantitative aspects of the problems. The remainder of this report will deal primarily with these simple cases in the hope that some better understanding of the phenomena may be attained.

ROTATION-INDUCED SECONDARY FLOWS

It is relatively easy to understand the qualitative behavior of rotation-induced secondary flows. However, the quantitative calculation of such flows starting from the boundary layer equations is generally not simple. In many cases, sufficient understanding may be gained from use of inviscid secondary flow theory. For example, in centrifugal rotors the major secondary flows often result from shroud boundary layers generated in the inducer section and/or other axial velocity profile nonuniformities (primary vorticity) that enter the impeller from upstream. When such effects are present, the streamwise (secondary) vorticity that develops downstream in the rotor depends to only a negligible extent upon local viscous effects.

It is not the intent of this paper to review inviscid theory in detail. Kramer and Stanitz (ref. 30) and Smith (ref. 44) develop the basic theory for application to incompressible fluids in rotating coordinates while Howard (ref. 24) extends it to simple compressible fluids. Application of the theory to real rotor flows appears to be rare, but there are useful exemplary calculations in references 30 and 44 and some attempts at prediction of real flows in centrifugal impellers in references 24 and 25.

In strictly axial-flow impellers, inviscid and viscous theory shows that coordinate rotation has no effect on the development of secondary vorticity in end-wall boundary layers. End-wall secondary flows develop due to the pressure field caused by turning the relative flow. However, secondary (radial) flows may develop on axial rotor blading as a consequence of coordinate rotation. In the latter case, because the layers generally start thin and grow in the chordwise direction, the full equations rather than inviscid theory should be employed.

The simplest case of rotation-induced secondary flow is the radial outflow in the boundary layer on a rotating disk. The laminar solution is well known, and since the classic stability and transition studies of Gregory, et al. (ref. 18), increasingly sophisticated solutions of the turbulent problem have become possible. The references to this problem are too numerous to list here, but useful solutions of the turbulent disk problem start with von Karman's paper (ref. 27) in 1921. A recent study on this topic, Cham (ref. 8), compares a variation of Head's entrainment method for solution of the three-dimensional turbulent boundary layer to

experiment. In comparison to the laminar flow solution, the most striking feature of the turbulent disk flow is the relatively small values of the secondary radial flow velocities.

Axial Rotor Blade Boundary Layers

Closely related to the simple disk flow problem are problems concerning boundary layers on axial-flow rotor and propeller blades. Because unstalled, axial rotor blade layers remain very thin, it has usually been assumed that the radial, secondary flows developed therein may be neglected. One of the first examinations of this rotational effect appears to be that of Banks and Gadd (ref. 2) who considered laminar and turbulent layers on rotating, helical surfaces, and the limiting case of sectors of flat circular disks, in an attempt to study viscous flow effects on ship propellers. Lakshminarayana (ref. 31) and Horlock (ref. 23) have recently reported work in progress for similar geometries. Figure 10 in reference 23 gives some calculated results for a segment of a disk where the boundary layer grows from its leading edge. It is shown there, as for full disk flows, that the secondary skewing of a turbulent layer is much less than that of a laminar layer. Similar results in reference 2 confirm this conclusion and, in addition, it is pointed out that unless the tangential flow tends to separate, or the tangential velocity profiles become quite distorted as a result of axial (chordwise) adverse pressure gradients, the radial flows will be very small for the turbulent case. For normal blade chord lengths and nonseparating turbulent conditions, the conventional neglect of this effect may indeed be justified.

On the other hand, if the flow is separating, or close to two-dimensional stall, the radial secondary flows may be important. Banks and Gadd (ref. 2) note the possibility that, as the chordwise profiles distort, the development of larger radial flows leads to a chordwise component of Coriolis force[6] that may be capable of "bucking" the adverse, chordwise pressure gradient and perhaps cause delay of two-dimensional, profile separation compared to an otherwise equivalent nonrotating flow. This rather surprising idea appears not to have been pursued too far in turbomachine flow research, although the authors of reference 2 say that the experiments of reference 22 on propeller lift coefficients tend to confirm this conclusion. It is believed that further work on this phenomenon could be justified. Experimental work would need to be done in a rotor as there appears to be no way to model the effect in a stationary system; i. e., a cascade.

---

[6] Believed to be the "coupling" effect mentioned by Horlock (ref. 23) as now under study.

Radial Passages, Tubes, and Ducts

Compared to axial flow rotors, blade passages in centrifugal impellers are more nearly like long ducts; that is, passages whose lengths are at least several times greater than their hydraulic diameters. As a consequence, boundary layers tend to be relatively thick compared to passage sectional dimensions and the secondary flows developed therein of considerable importance. In this section, we shall briefly review some basic results on flow in long tubes and ducts that rotate steadily about axes perpendicular to the main flow, x, direction (see fig. 3). Most studies that are of more than qualitative value have confined consideration to very long ducts where the flow is fully developed, or nearly so. The recent study by Moore (ref. 37) is a notable exception and will be discussed at the end of this section.

Laminar flow in long, rotating ducts has been analyzed for two limiting cases: (1) very small rotational speed ($Ro \ll 1$) and (2) large rotational speeds ($Ro \gg 1$). The latter case (see refs. 5 and 6) is of little interest in turbomachine applications, but the former, studied by Barna (ref. 3) and Benton (ref. 4), is of interest. For case (1), when the channel rotation number, $Ro_c \triangleq 2\omega D/\bar{u}_m$, or tube number, $Ro_d \triangleq \omega d/\bar{u}_m$, is small, the experimental results of Trefethen (refs. 47 and 48) on round tube flows and the recent work by Moore (ref. 36) on turbulent flow in rectangular ducts may profitably be reviewed.

As shown in references 3 and 4, the fully developed, laminar flow in round tubes is a small perturbation on Hagen-Poiseuille flow for $Ro \ll 1$. Counter-rotating, secondary flows develop above, and below, the plane which divides the tube and is perpendicular to the axis of rotation. The

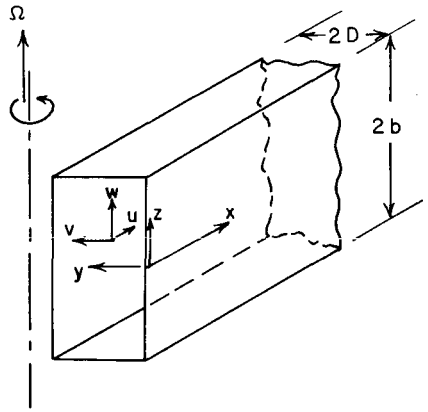

FIGURE 3.—*Rotating rectangular channel.*

additional dissipation engendered by the secondary motions results in an increase of the friction factor, $\hat{f}$. To first order, the ratio $\hat{f}/\hat{f}_0$ (friction factor to the zero-rotation friction factor) was found to be simply related to the parameter $Re_h\sqrt{Ro_d}$. Experimentally, Trefethen (refs. 47 and 48) essentially confirmed this result, but best agreement with his data that span the range $2\times10^2<Re_h\sqrt{Ro_d}<3\times10^3$ fits the formula

$$\frac{\hat{f}}{\hat{f}_0}=0.20(Re_h\sqrt{Ro_d})^{0.4}$$

The data become nearly tangent to Barna's linearized theory for $Re_h\sqrt{Ro_d}=3\times10^3$. Clearly, the secondary flows generated by rotation can significantly affect laminar friction factors in long, round tubes.

In most rotor flows the small rotation condition, $Ro<1$, should hold, but laminar flow is unlikely because of the high Reynolds numbers. Furthermore, passages are generally rectangular rather than round. Turbulent friction factors for round tubes are presented in references 47 and 48 and by Moore (ref. 36) for rectangular ducts (fig. 3) of aspect ratios: $AS\triangleq b/D=\frac{1}{2}:1$, 1:1, 4:1 and $7\frac{1}{3}:1$. These results show that for values of $Ro_c\lesssim0.05$, which are typical in practice, the rotation may increase friction factors by $\sim$20 percent at most. Moore's results for $AS=1:1$, as one might expect, were consistent with those for round tubes. However, the uncertainty in the data is too high to allow recommendation of formulas for $\hat{f}/\hat{f}_0$.

Moore's results (ref. 36) and similar related experiments (refs. 21 and 35) contain measurements of mean velocity profiles, wall shear stress, and turbulence, $\overline{u'^2}$, profiles measured at the duct center plane (see ℄ in fig. 4) in addition to friction factor data. Only the wall skin friction coefficient, c_f, data at the symmetry plane will be discussed. These data were obtained by the Preston tube method for a range of Reynolds numbers, $Re_h\approx1.3$ to 3.9×10^4 and rotation numbers up to $Ro_c\approx0.05$ for each of the four channels. The data are plotted in figure 5 as $c_f/(c_f)_0$ versus channel aspect ratio. Channel trailing (suction) side wall stress is seen to be lower, and leading (pressure) side stress higher than the no-rotation stress at the same aspect ratio and Reynolds number. The effect of rotation decreases with increase of aspect ratio, but at all aspect ratios except 1:1 on the trailing side, increasing rotational speed increases the deviation of c_f from its no-rotation value.

As pointed out by Moore (ref. 36), these trends appear to be primarily associated with the secondary flow patterns developed in the channel. Figure 4 indicates typical qualitative secondary streamline patterns for ducts of low and high aspect ratio. Clearly the flow of energy-deficient fluid from the end walls to the trailing surface and the return flow near the channel center plane should be more important at low than at high aspect ratios. End wall regions are a less important fraction of the flow

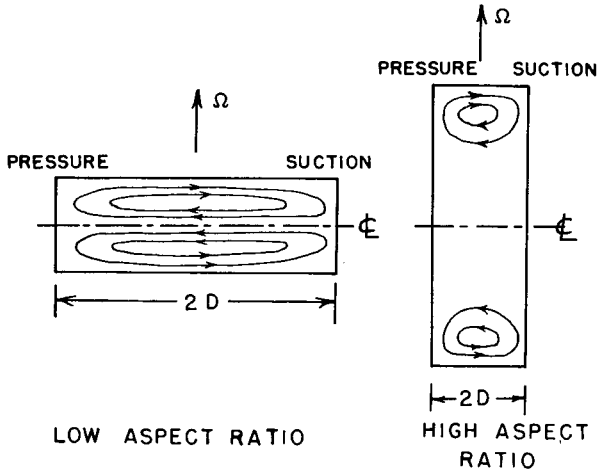

FIGURE 4.—*Secondary-flow streamlines in long rotating channels.*

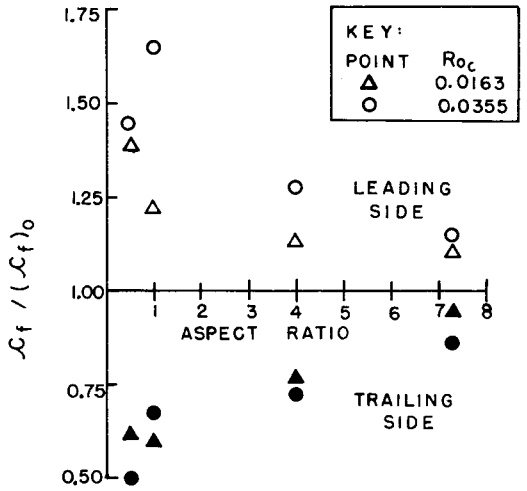

FIGURE 5.—*Skin friction coefficient versus channel aspect ratio; data of reference 36, figure 18.*

field and further removed from the center plane at high aspect ratio. In the limit, as $AS \rightarrow \infty$, secondary flow theory would result in the prediction that $c_f/(c_f)_0 = 1$ independent of channel rotational speed. Moore's results (those of fig. 5 and others) are clear proof that rotation-induced secondary flow plays a very important role in the fluid dynamics of turbulent passage flows, particularly in ducts of low aspect ratio. However, the effects of stability must also be considered. It is my belief that at $AS = 7\frac{1}{3}:1$ the

effects noted by Moore are dominated by the stability of the flow and hardly influenced by secondary flow except near the duct end walls. Demonstration of this conclusion will be discussed in the section on turbulent channel flow–experimental results.

The only known complete study of the effects of secondary flow in a passage that is in any way closely comparable to a radial-flow centrifugal impeller passage is that of Moore (ref. 37). He conducted low-speed, air-flow experiments centered on study of the developing side-wall turbulent boundary layers in a rotating, radial, two-dimensional diffuser of 15° included angle between the leading and trailing sides. Boundary layers were thin at channel inlet on all walls, and the core of the flow was irrotational in stationary coordinates; i.e., $\bar{\xi}_{abs}=0$. In addition, he computed the end-wall and side-wall layers using a known turbulent layer method[7] modified to include the rotation-driven secondary flows. His procedure included a simple momentum transport theory for the corner regions and simultaneous computation of the core flow. The results indicate that secondary flow from pressure to suction side significantly alters the development of all boundary layers. The pressure (leading) and end-wall layers are thinned and the suction-side layer thickened even though the potential core flow region imposes more adverse pressure gradient on the pressure-side layer than on the suction-side layer. A large "wake" region develops downstream on the suction side. It appears to be fed by the end-wall cross flows and has little or no backflow. In addition, the wake shear layer seems to be unusually quiescent with little mixing as might be expected from the stabilizing influence of rotation.

The agreement between theory and experiment in this case (ref. 37) is quite reasonable and leads one to hope that one may eventually apply three-dimensional turbulent boundary layer theory to more realistic impeller design problems. Of course, in many real situations the inlet conditions and channel geometry will considerably complicate the situation (see the introduction to this section).

BOUNDARY LAYER STABILITY AND TURBULENCE

To limit discussion, the remarks of this section will be confined to flows that are incompressible, steady and two-dimensional in the time mean, and in which the mean relative velocity lies in planes perpendicular to the axis of system rotation. Three-dimensional fluctuation and steady perturbations that do not arise as a consequence of end walls must, however, be allowed. In addition the mean flow will be assumed parallel, or

[7] Similar to the Moses method (see ref. 49).

nearly parallel (boundary layer), shear flow (see fig. 2). The Cartesian components of velocity are

$$u=\bar{u}+u'$$

$$v=\bar{v}+v'$$

$$w=\bar{w}+w'$$

Here $\bar{v}\ll\bar{u}$ and $\partial(\overline{\ })/\partial x\ll\partial(\overline{\ })/\partial y$ are the boundary layer assumptions. $\bar{w}=0$ and $\partial(\overline{\ })/\partial z=0$ limit the mean flow to be two-dimensional.

The time mean boundary layer equations obtained from equations (22) and (28) and these assumptions are

$$\bar{u}\frac{\partial\bar{u}}{\partial x}+\bar{v}\frac{\partial\bar{u}}{\partial y}=-\frac{1}{\rho}\frac{\partial\overline{p^*}}{\partial x}+\nu\frac{\partial^2\bar{u}}{\partial y^2}+\frac{1}{\rho}\frac{\partial(-\rho\overline{u'v'})}{\partial y} \tag{4}$$

in the x-direction, and

$$2\Omega\bar{u}=-\frac{1}{\rho}\frac{\partial\overline{p^*}}{\partial y}-\frac{\partial(\overline{v'^2})}{\partial y} \tag{5}$$

in the y-direction. The time mean continuity equation is

$$\frac{\partial\bar{u}}{\partial x}+\frac{\partial\bar{v}}{\partial y}=0 \tag{6}$$

If $\overline{p_a^*}$ is the value of $\overline{p^*}$ at a plane $y=a$ where $\overline{v'^2}=\overline{v_a'^2}$, equation (5) can be integrated at any x-station to obtain

$$-\frac{1}{\rho}\overline{p^*}=-\frac{1}{\rho}\overline{p_a^*}+2\Omega\int_a^y\bar{u}\,dy+(\overline{v'^2}-\overline{v_a'^2})$$

This equation is then differentiated with respect to x and substituted into equation (4) to give

$$\bar{u}\frac{\partial\bar{u}}{\partial x}+\bar{v}\frac{\partial\bar{u}}{\partial y}=-\frac{1}{\rho}\frac{d\overline{p_a^*}}{dx}+2\Omega\int_a^y\frac{\partial\bar{u}}{\partial x}\,dy-\frac{d\overline{v_a'^2}}{dx}$$

$$+\frac{\partial\overline{v'^2}}{dx}+\nu\frac{\partial^2\bar{u}}{\partial y^2}+\frac{1}{\rho}\frac{\partial}{\partial y}(-\rho\overline{u'v'}) \tag{7}$$

which reduces the mathematical description to two equations, (6) and (7). For a boundary layer, $\overline{p_a^*}$ and $\overline{v_a'^2}$ are presumably given functions of x in the free stream, or at a wall. For turbulent flow, additional input is, of course, required to describe $\overline{v'^2}$ and $\overline{u'v'}$.

Before proceeding to the discussion on fully turbulent and relaminarizing flows in rotating channels, it will be useful to review briefly some laminar flow stability results obtained by linearized small disturbance theory.

It is hoped thereby to demonstrate the pertinence and utility of the Richardson number and other rotation parameters.

Laminar Stability

The stability of plane, rotating, laminar shear flows has been examined by several investigators (refs. 10, 34, and 39) and is currently under investigation by our group (ref. 50). All this work utilizes linear stability theory and hence the results do not purport to predict laminar-turbulent transition.

In an early effort, Conrad (ref. 10) investigated the stability of the Blasius boundary layer on curved or flat rotating surfaces. He recognized, as did Mellor (ref. 34), that the system rotation and wall curvature terms that enter the linearized stability equations (Orr-Sommerfeld type) have no effect on the growth or decay of pure, two-dimensional disturbances such as Tollmien-Schlichting (T-S)[8] waves. However, the stability of the flow to longitudinal vortex cells of the Taylor-Görtler (T-G)[8] type is affected by rotation. Conrad assumed disturbances of the T-G type and obtained a solution that was unstable to cells of all wave lengths, λ, but most unstable to those of $\lambda \to \infty$. Considering only layers on flat rotating walls, the Reynolds numbers required for instability were found to be

$$Re_\delta \geqq \frac{8.8}{\sqrt{Ro_\delta}}$$

where the thickness δ in the parameters is the 99 percent boundary layer thickness of a Blasius layer. It is now known that this solution is valid only for $| Ro_\delta | \ll 1$, as terms required for complete solution were dropped before linearization of the stability equations. A leading side flow corresponds to positive values of Ro_δ and may be unstable to T-G disturbances, but a trailing side flow is stable as shown by the solution above where only imaginary Reynolds numbers result when Ro_δ is negative.

Recently, Potter and Chawla (ref. 39) have investigated the stability of the Blasius layer on flat rotating walls using a general disturbance perturbation containing both T-S waves and T-G cells. Their work complements and extends Conrad's work, although they did not examine the pure T-G cell problem.

We have found a simpler problem for which the T-G disturbance solution is completely known for all values of Ro: the simple Couette flow between flat, parallel walls, one of which is sliding at speed U (see fig. 6). The exact analogue of this problem is the thermal instability problem of Bénard as solved in reference 9. From that solution, the most unstable

[8] For brevity, the abbreviation T-S will be used for Tollmien-Schlichting waves and T-G for Taylor-Görtler cells.

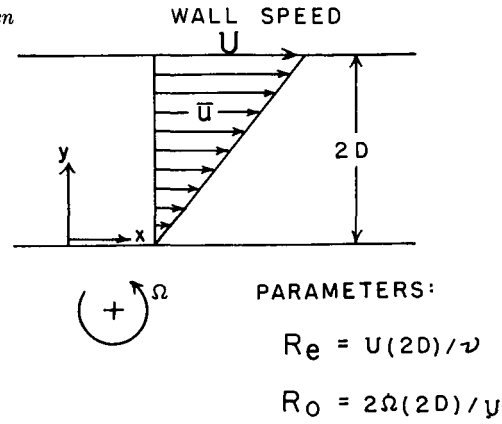

FIGURE 6.—*Couette flow between rotating channel walls.*

T-G cell has a wave length $\lambda = 2.02\ (2D)$ for which the critical Reynolds number ($Re \triangleq 2DU/\nu$) is

$$(Re)_{crit} = \frac{41.3}{\sqrt{Ro(1-Ro)}} = \frac{41.3}{\sqrt{-Ri}}$$

where $Ro \triangleq 2\Omega(2D)/U$. For this flow the local profile stability parameter, the gradient Richardson number, is a constant as $Ro = -S$ and hence $Ro(1-Ro) = -Ri$. The flow is always stable for $Ri > 0$, and tends to be unstable for $Ri < 0$. For the particular condition where $Ro = -S = \frac{1}{2}$, Ri obtains its minimum value of $-\frac{1}{4}$, for which the minimum value of the critical Reynolds number becomes 82.6. At all other positive values of Ro, values of Re larger than 82.6 are required for instability.

We (ref. 50) have also examined the stability of laminar, fully developed flow in a rotating channel (fig. 7). The mean profile is parabolic and unaffected by rotation in this case (see the section on turbulent channel flow—theoretical considerations). The linear stability equations contain all rotation effects in a gradient Richardson number term, but, as $d\bar{u}/dy$ varies with y, the Richardson number is not a constant for the flow. With the assumption of T-G cell disturbances, numerical solution has yielded a minimum critical Reynolds number of $(Re)_{crit} = 88.7$ at a channel rotation number of $Ro_c = 0.5$. The Reynolds number is defined here as $Re = 2D\bar{u}_m/\nu$. The critical wavelength of the cell was computed as $\lambda = 1.28D$. The equations show that complete stability must occur for $Ro_c \geqq 3$, in which case the gradient Richardson number is greater than or equal to zero at all points in the flow.

As already pointed out, rotation does not affect stability of the flow to purely two-dimensional disturbances such as waves of the T-S type. If

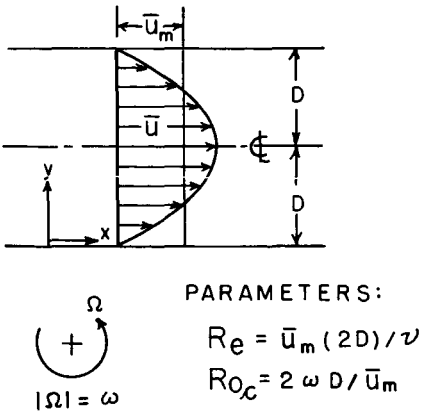

FIGURE 7.—*Fully developed, laminar flow in a rotating channel.*

rotational speeds are very high, the Taylor-Proudman theorem indicates that three-dimensional disturbances are not possible. For example, T-G-type cells should be highly damped for large values of *Ro*. Hence, one might conclude that, even though two-dimensional disturbances may amplify in a rotating shear flow, the three-dimensionality required for breakdown of the flow to turbulence may be inhibited by rotation. If *Ro* is large enough, true turbulence may never occur in rotating flow. Certainly, one can expect to see a significant effect of rotation on the laminar-turbulent transition. Linear stability theory provides at least a guide and some feeling for the important physical parameters such as the gradient Richardson number which may, in part, control the transition process.

Turbulent Channel Flow—Theoretical Considerations

Under the conditions stated in the introduction to this section, the appropriate boundary layer equations are (6) and (7). If, in addition, the flow is fully developed between the parallel side walls of a channel where the end walls are very far apart ($b \to \infty$, fig. 3) then $\bar{v}=0$ and $\partial\bar{u}/\partial x=0$, etc. From equation (7) we obtain

$$\frac{d\overline{p_a}^*}{dx} = \frac{d\tau}{dy} = \text{constant} \tag{8}$$

where the total fluid shear stress

$$\tau = \nu\rho\frac{d\bar{u}}{dy} + (-\rho\overline{u'v'}) \tag{9}$$

Equation (8) shows that τ is a linear function of y as it is in stationary coordinates.[9] However, as will become evident shortly, the linear τ function is not generally symmetrical about the channel centerline, and we can expect $|\tau_T|$, the trailing (suction) side wall shear stress magnitude, to be less than $|\tau_L|$, the leading (pressure) side wall shear stress magnitude (see fig. 8). For small Ro_c, experiments (ref. 19) on turbulent channel flow indicate that the slope of the τ function is not affected by rotation and hence the channel pressure drop is dependent on Reynolds number alone, even though the wall stresses depend on rotation. In this section, qualitative explanation of these phenomena will be attempted.

Our approach is to start from the equations for the rate of generation (evolution or advection) of components $\overline{u'^2}$, $\overline{v'^2}$, and $\overline{w'^2}$ of the turbulence energy, $2\overline{q'^2}$, and Reynolds stress, $-\rho\overline{u'v'}$, as one follows a mean streamline; i.e., the equations for

$$\frac{D(\overline{u_i'u_j'})}{Dt} \triangleq \frac{\partial(\overline{u_i'u_j'})}{\partial t} + \bar{u}_l \frac{\partial(\overline{u_i'u_j'})}{\partial x_l} \tag{10}$$

in their special form for channel flow. Townsend (ref. 46) derived these equations for zero rotation and they were extended by Halleen and Johnston (ref. 19) to rotating flows. The extended equations differ from

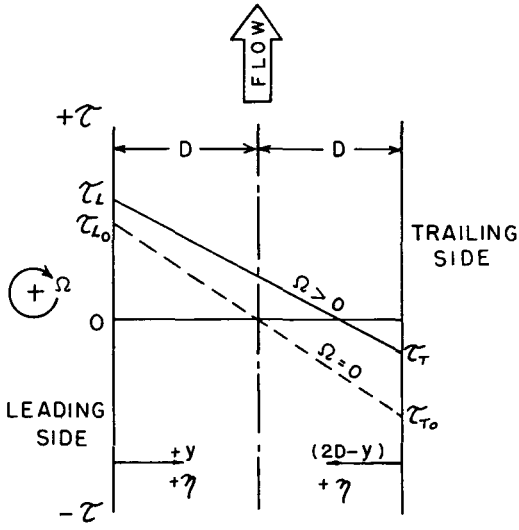

FIGURE 8.—*Shear stress distributions in fully developed channel flow; solid line for turbulent or mixed flow; dashed line also valid at all Ω with plane laminar flow.*

[9] If the flow is laminar ($u'=v'=w'=0$), τ is symmetrical about $y=D$, and equations (8) and (9) give a symmetrical, parabolic $\bar{u}$ velocity profile which is independent of rotational speed.

those of Townsend only by an additional rotation-induced turbulence production term. The total, general rate of production of turbulence term is

$$P_{ij}=(-\overline{u_i'u_l'})\frac{\partial \bar{u}_j}{\partial x_l}+(-\overline{u_j'u_l'})\frac{\partial \bar{u}_i}{\partial x_l}-[\overline{u_i'f_j'}+\overline{u_j'f_i'}] \tag{11}$$

f_i' and f_j' are the fluctuating parts of the Coriolis acceleration term (see eq. 24). Hence, the rotational production terms are those in the square set of brackets. The full equations are shown as (12) in table I, as are their special forms for fully developed channel flow, equations (13) through (17).

First, consider equation (13) for $\overline{u'^2}$ and equation (14) for $\overline{v'^2}$. For positive rotation Ω and stress $-\overline{u'v'}$, production of the streamwise component $\overline{u'^2}$ is inhibited by rotation, whereas production of the transverse component $\overline{v'^2}$ is enhanced. This set of circumstances occurs near the leading (pressure) side of the channel. The reverse situation holds near the trailing (suction) side where $-\overline{u'v'}$ is negative (see fig. 8). Although the rotation Ω does not appear explicitly in the turbulence energy equation (eq. (16)) that is obtained by summing equations (13), (14), and (15), the fact that it affects the production rates of the components of $\overline{q'^2}$ shows that rotation plays a role in the establishment of the turbulence field.

The direct influence of rotation on turbulent stress $-\rho\overline{u'v'}$ is seen in equation (17), the equation for $-\overline{u'v'}$. Bradshaw (ref. 7) indicates that the effects of rotation are best illustrated by taking the ratio of (minus) the rotation production induced by $\overline{u'^2}$ to the production induced by $\overline{v'^2}$ This ratio, called the stress Richardson number, is

$$Ris=\frac{\overline{u'^2}}{\overline{v'^2}}\frac{-2\Omega}{(d\bar{u}/dy)-2\Omega}=\frac{\overline{u'^2}}{\overline{v'^2}}\frac{S}{S+1} \tag{18}$$

Except for the factor $\overline{u'^2}/\overline{v'^2}$,which in a boundary layer is roughly equal to or less than 4, *Ris* is equal to a flux Richardson number obtained by forming (minus) the ratio of total production of $\overline{v'^2}$ (eq. (13)) to total production of $\overline{u'^2}$ (eq. (14)); i.e.,

$$Rif=\frac{-2\Omega}{(d\bar{u}/dy)-2\Omega}=\frac{S}{S+1} \tag{19}$$

Both these ratios, in a sense, express the ratio of $-\overline{u'v'}$ production due to rotation to that caused by absolute vorticity, $\bar{\xi}_{abs}$. Hence, in a region where $\bar{\xi}_{abs}=0$ all production, if any, is caused by system rotation. Close to

TABLE I.—*Turbulence Energy Equation in Rotating Frame for General and Fully Developed Channel Flow Case*

Equation number	Generation along mean streamline	= Turbulence production: (Mean flow shear production)	+ Turbulence production: (Rotation induced production)	+ Turbulent field convective transport: (diffusion)	+ Turbulent velocity pressure fluctuation interaction: (pressure-strain)	+ Viscous turbulent field interaction: (shear work) and (dissipation)	Description of terms
(12)	$\frac{D(\overline{u_i'u_j'})}{Dt}$ (equation (10))	$(-\overline{u_i'u_l'})\frac{\partial \bar{u}_j}{\partial x_l}$ $+(-\overline{u_j'u_l'})\frac{\partial \bar{u}_i}{\partial x_l}$	$-[\overline{u_i'f_j'}+\overline{u_j'f_i'}]$	$-\frac{\partial}{\partial x_l}(\overline{u_i'u_j'u_l'})$	$-\frac{1}{\rho}\left(\overline{u_i'\frac{\partial p'}{\partial x_j}}+\overline{u_j'\frac{\partial p'}{\partial x_i}}\right)$	$\nu\left(\overline{u_i'\frac{\partial^2 u_j'}{\partial x_l^2}}+\overline{u_j'\frac{\partial^2 u_i'}{\partial x_l^2}}\right)$	General equation for ρ = constant Newtonian fluid with steady Ω
			Equations for fully developed channel flow				
(13)	0	$2(-\overline{u'v'})\frac{d\bar{u}}{dy}$	$-4(-\overline{u'v'})\Omega$	$-\frac{d}{dy}(\overline{u'^2v'})$	$-\frac{2}{\rho}\overline{u'\frac{\partial p'}{\partial x}}$	$\nu\frac{d^2\overline{u'^2}}{dy^2}-2\nu\overline{\left(\frac{\partial u'}{\partial x_l}\right)^2}$	Equation for $\overline{u'^2}=\overline{u_{11}^2}$ (streamwise)
(14)	0	0	$+4(-\overline{u'v'})\Omega$	$-\frac{d}{dy}(\overline{v'^3})$	$-\frac{2}{\rho}\overline{v'\frac{\partial p'}{\partial y}}$	$\nu\frac{d^2\overline{v'^2}}{dy^2}-2\nu\overline{\left(\frac{\partial v'}{\partial x_l}\right)^2}$	Equation for $\overline{v'^2}=\overline{u_{22}^2}$ (transverse)

(15)---	0	0	0	$-\frac{d}{dy}(\overline{w'^2v'})$	$-\frac{2}{\rho}\overline{w'\frac{\partial p'}{\partial z}}$	$\nu\frac{d^2\overline{w'^2}}{dy^2}-2\nu\overline{\left(\frac{\partial w'}{\partial x_l}\right)^2}$	Equation for $\overline{w'^2}=\overline{u_{33}'^2}$ (spanwise)
(16)---	0	$(-\overline{u'v'})\frac{d\bar{u}}{dy}$	0	$-\frac{d}{dy}(\overline{q'^2v'})$	$-\frac{1}{\rho}\frac{d}{dy}(\overline{p'v'})$	$\nu\frac{d^2\overline{q'^2}}{dy^2}-e$	Turbulence energy equation
(17)---	0	$(\overline{v'^2})\frac{d\bar{u}}{dy}$	$(\overline{u'^2}-\overline{v'^2})2\Omega$	$\frac{d}{dy}(\overline{u'v'^2})$	$\left(\overline{u'\frac{\partial p'}{\partial y}}+\overline{v'\frac{\partial p'}{\partial x}}\right)\frac{1}{\rho}$	$-\nu\frac{d^2(\overline{u'v'})}{dy^2}$ $+2\nu\overline{\left(\frac{\partial u'}{\partial x_l}\right)\left(\frac{\partial v'}{\partial x_l}\right)}$	Principal Reynolds stress equation $(-\overline{u'v'})=(-\overline{u_1'u_2'})$

the walls, in the inner layers where

$$\left|\frac{d\bar{u}}{dy}\right| \gg |2\Omega| \qquad \text{or} \qquad S \ll 1$$

one can conclude that $Ris \approx 4S$, $Rif = S$, and in addition the local stability parameter, the gradient Richardson number, $Ri = S$. Hence, in the wall layers, production of turbulent stress is enhanced by rotation where flow instability ($Ri < 0$) is indicated and reduced where stability ($Ri > 0$) is indicated by rotation.

These conclusions do not prove that shear stress magnitude will be greater near the leading side of the channel than near the trailing side. However, the demonstrated tendency of rotation to modify stress production in localized regions of the flow indicates that some excess, or deficit, of $-\rho\overline{u'v'}$ may occur in the layers where production is greater, or less, than that occurring under equivalent zero-rotation conditions.

Turbulent Channel Flow—Experimental Results

At Stanford, we have been studying the effects of rotation on turbulent, fully developed flow of water in a long channel of high aspect ratio, $AS = 7\frac{1}{3}:1$. The first results were reported by Halleen and Johnston (ref. 19). These consisted principally of dye flow visualization of the wall (sub)-layer structure (e.g., see ref. 29), measurements of wall shear stress, primarily by the Preston tube method, and measurement of the mean velocity profiles at the channel centerline (see ¢ in fig. 4). Recent work includes continued analysis of these earlier results and extensive new flow visualization work using the hydrogen bubble technique (ref. 50).

The results to be discussed were obtained far enough downstream in the channel ($x/D = 58$ and $x/D = 68$) so that the flow was quite close to fully developed. Reynolds numbers, Re_h, from 5×10^3, where fully turbulent flow is barely maintained at zero rotation, up to 6×10^4 were used, and a range of rotation numbers, Ro_c, as high as 0.2 at low Reynolds number and 0.08 at $Re_h = 6 \times 10^4$ were achieved in these studies.

Early in the program, the visual studies of the wall layers showed that the flow in the central regions of the wide ($2b = 11$ inches) side walls was not significantly affected by secondary flows from the narrow ($2D = 1.5$ inches) end walls. Hence, the conclusions and results to be discussed below are felt to be essentially independent of end-wall effects.

The two principal conclusions of the visual studies[10] are

(1) Rotation suppresses turbulence production on the trailing (suction) side of the channel as anticipated. At sufficiently high Ro_c, complete laminarization of the trailing side wall layers was observed.

---

[10] See Fluid Mechanics Research Film No. J-1, by Halleen and Johnston, Engineering Societies Library, New York.

(2) On the leading (pressure) side, it was difficult to observe the predicted increase of small-scale turbulence, but a new, large-scale structure in the form of Taylor-Görtler-like cells with their axes aligned in the mean flow direction was seen to appear at higher rotational speeds.[11]

Some of the evidence for these conclusions and some other observations are presented below.

Figure 9 shows a sequence of photographs of hydrogen bubble timelines generated on a wire mounted very close and parallel to the trailing wall and perpendicular to the oncoming mean flow (left to right). The Reynolds number was fixed at $Re_h = 1.5 \times 10^4$, and each picture represents conditions at successively higher Ro_c values. As Ro_c increases, the trailing wall layer structure progresses from a fully turbulent streak structure (see ref. 29) at $Ro_c = 0$ to a partly laminar structure at $Ro_c = 0.107$.

Visual data of this type, and the earlier dye studies, allowed the construction of a flow regime map for the trailing side (fig. 10). In the region below the band of points, the flow was judged to be fully turbulent, but for Ro_c values at, and just above, the band the wall layer is so stable that

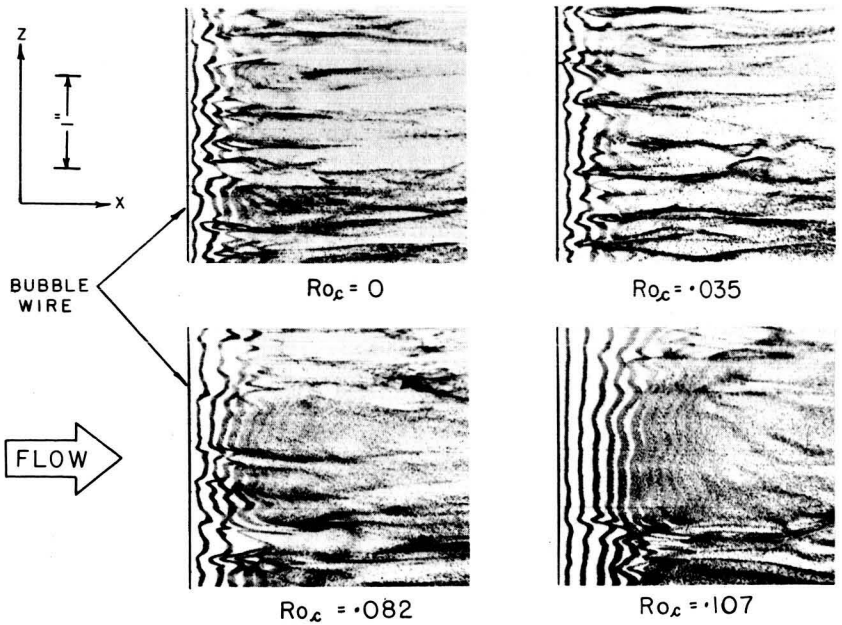

FIGURE 9.—*Hydrogen bubble time lines on channel trailing side,* $Re_h = 15\,000$, *by D. K. Lezius in 1969. (ref. 50).*

[11] T-G-type vortices have been observed in other turbulent flows such as cases with wall curvature (refs. 28, 38, and 43).

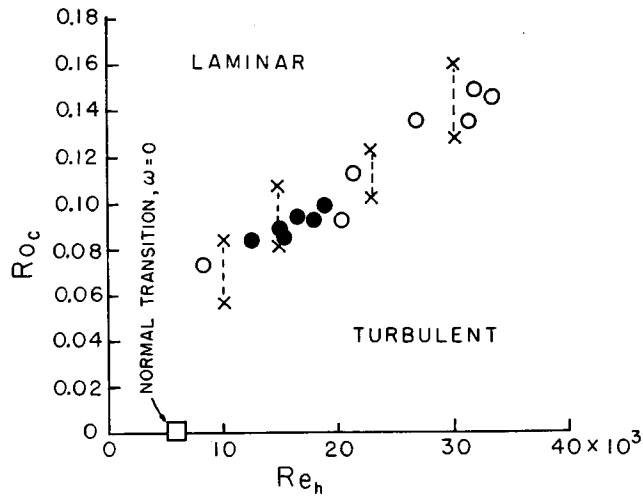

FIGURE 10.—*Wall-layer flow regime line on trailing side—circles from dye studies (ref. 19), open points stationary observer, closed points rotating observer; cross points from film scenes of H_2 bubbles by D. K. Lezius in 1969. (ref. 50).*

it could be called "laminarized." For very large Ro_c the wall layers on the trailing side were completely laminar.

Figure 11 is an attempt to qualitatively illustrate the leading side flow regime. In the early work (ref. 19) the existence of the vortex cells was deduced from the observation of regions of dye concentration (re-collection) near the center of the channel. The dye was injected slowly and uniformly along a spanwise slot at the wall, swept in the wall layers toward the region adjoining two cells, and then ejected away from the wall to form the region of re-collection above the cells. This vortex cell structure has been confirmed in recent hydrogen bubble pictures. It should be noted that these cells are not stationary in time and space once formed, but they shift sideways, disappear, and reform in an irregular way if the flow is viewed for a sufficient period of time.

Mean velocity profiles from reference 19 are shown in figures 12 and 13 for $Re_h \approx 6 \times 10^4$ and figure 14 for $Re_h \approx 2 \times 10^4$ on the trailing side. The considerable reduction in velocity gradients on the trailing side, and increase on the leading side, as rotation number increases is evident. As will be shown shortly, these changes are not just due to rotation-induced changes in shear stress, but also result from changes of mixing length (or eddy viscosity). At the lower Reynolds number (fig. 14), the shapes of the trailing side mean velocity profiles for $Ro_c \geqq 0.111$ show no resemblance to the standard turbulent law of the wall profile. At the highest Ro_c, the profile is nearly like the parabolic shape characteristic of laminar

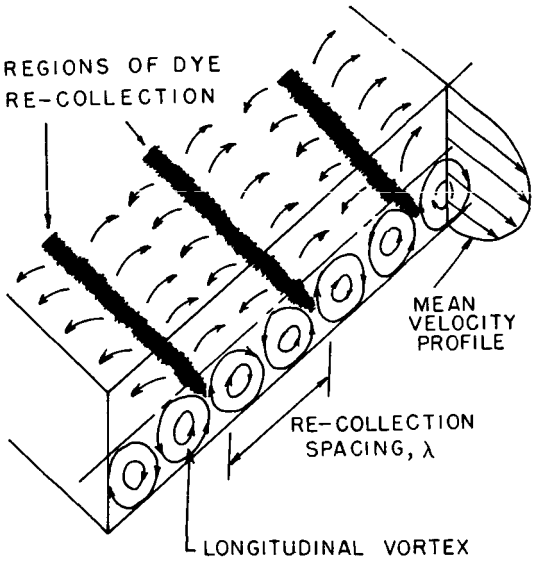

FIGURE 11.—*Longitudinal large vortex structure near leading wall; from reference 19.*

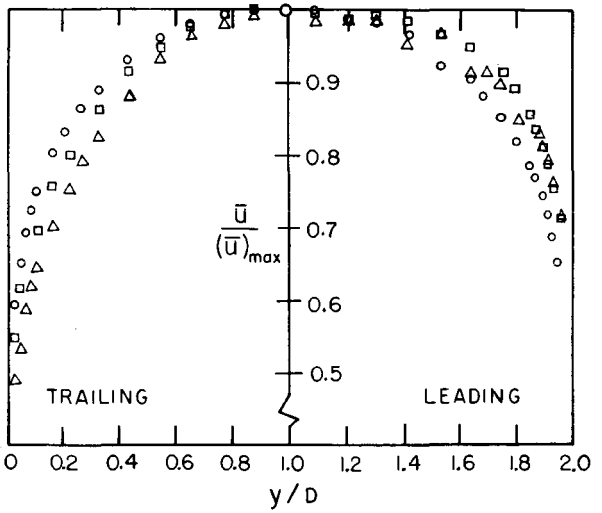

KEY:	POINT	Ro_c	Re_h	X/D
	○	0	57,200	68
	□	0.044	57,700	68
	△	0.083	60,400	68

FIGURE 12.—*Mean velocity profiles; rotating channel flow data of reference 19.*

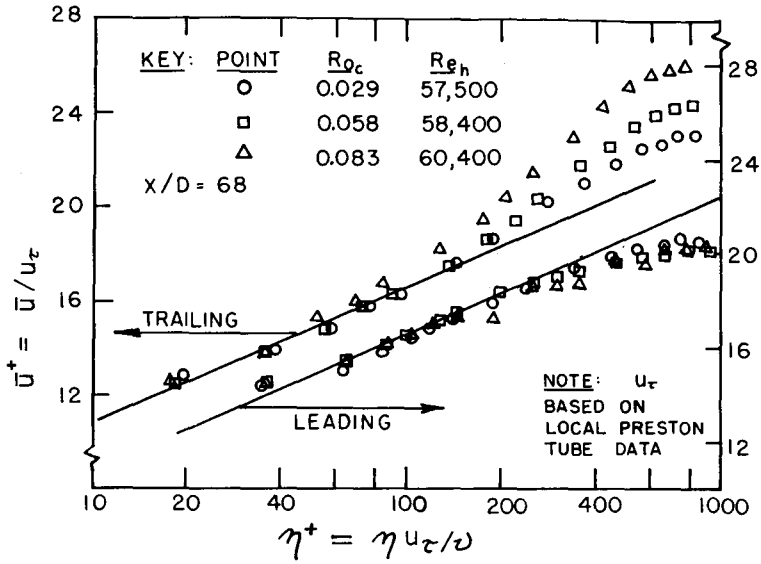

FIGURE 13.—*Mean velocity profiles; rotating channel flow data of reference 19; lines are* $5.8 \log_{10} \eta^+ + 5.0$ *fit to data at* $\mathrm{Ro_c} = 0$.

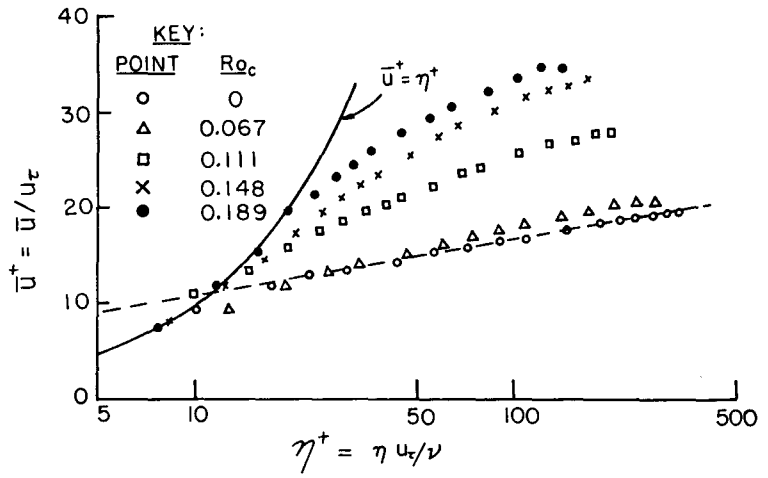

FIGURE 14. *Mean velocity profiles on trailing side of rotating channel,* $\mathrm{Re_h} = 20\,000$, $\mathrm{x/D} = 68$; *data of reference 19.*

flow. This is further confirmation of the trailing side "laminarization" noted in the visual studies.

The Preston tube measurements of wall shear stress expressed as the ratio of wall shear velocity to zero-rotation wall shear velocity are plotted against rotation number in figure 15. Moore's data (ref. 36) for his $7\frac{1}{3}$:1

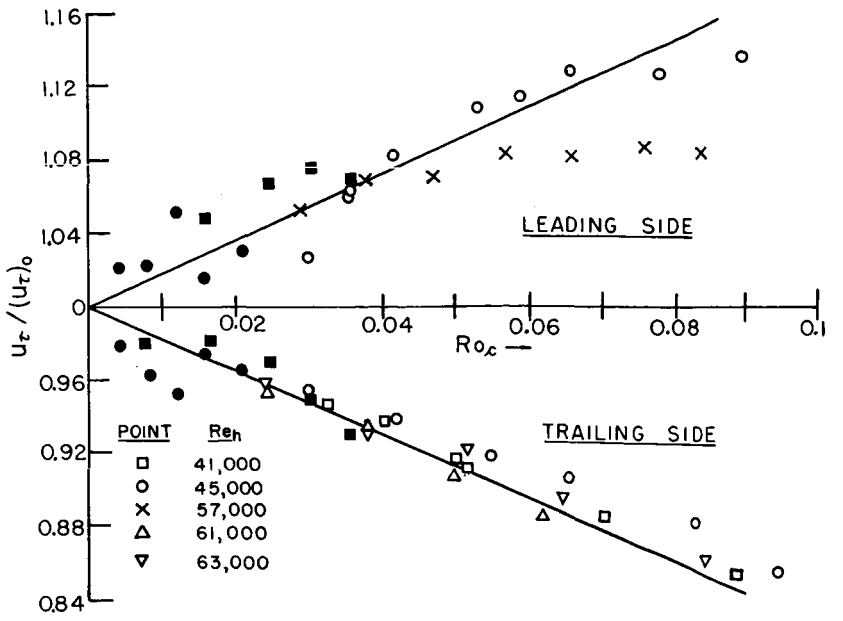

FIGURE 15.—*Ratio of wall shear velocity to zero-rotation wall shear velocity; open symbols from reference 19, closed symbols from reference 36.*

aspect ratio channel are also presented and appear to be in fair agreement with the data of reference 19. Since it has been shown that rotation changes the turbulence structure significantly for the Halleen and Johnston data, and that end-wall secondary flow was probably not significant in the region of measurement, the results of figure 15 bear up the previous conclusion that, at the higher aspect ratios, Moore's results reflect the effect of structure change rather than secondary flow.

An interesting feature of figure 15 is the apparent leveling out of the leading side u_τ values above some moderate value of Ro_c. This effect is believed to be a reflection of the onset of the large-scale longitudinal vortex structure on the leading side of the channel, but the matter is still under investigation.

The experimental data of Halleen and Johnston (ref. 19) are sufficient for the determination of the distribution of mixing length, l (or eddy viscosity), distribution for the channel. Mixing length was determined from these data, using the definition of l

$$l \triangleq \frac{\sqrt{\tau/\rho}}{(d\bar{u}/d\eta)}$$

where the τ-distribution for fully developed flow (fig. 8) was assumed to

fit between the measured values of wall shear stress. $d\bar{u}/dy$ was determined graphically from the measured mean velocity profiles.

The zero-rotation mixing lengths, l_0, are plotted in figure 16. At $Re_h = 2 \times 10^4$, it became evident from comparison of results at $x/D = 58$ and $x/D = 68$ that the flow in the channel was probably not quite fully developed. Hence, the results shown in figures 17 and 18 were only plotted for points of η less than $\sim$0.04 ft, where the shear stress distribution assumption was felt to be valid.

The ratio l/l_0 is plotted as a function of gradient Richardson number, Ri, with Ro_c and Re_h as parameters in figures 17 and 18. The only data shown are for the case where the whole channel flow was turbulent. Furthermore, no data points for η^+ less than $\sim$50 were included, as these points lay in, and close to, the wall layers which could be partially laminar.

These figures show clearly that mixing length (and eddy viscosity) is reduced near the trailing wall (fig. 17) and increased near the leading wall (fig. 18). Although the accuracy of the results is not better than ± 10 percent, it is believed that, at least near the trailing side, the separate influence of the global parameter Ro_c as well as the local variable Ri can be seen.

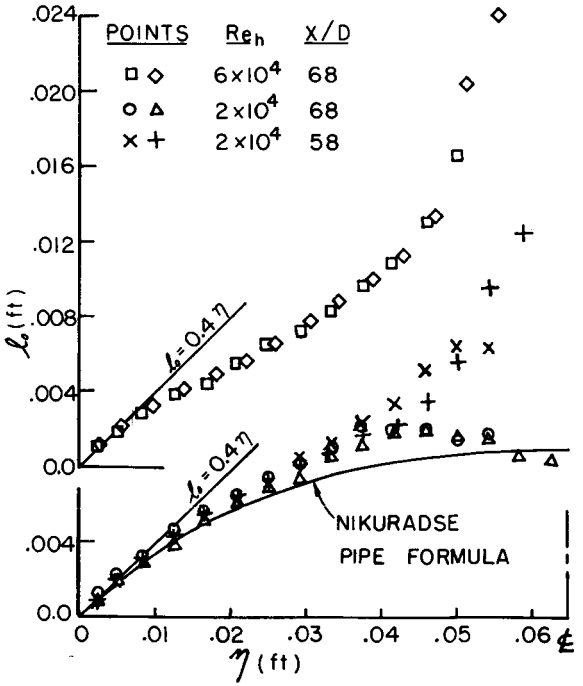

FIGURE 16.—*Zero-rotation mixing length profiles from data of reference 19.*

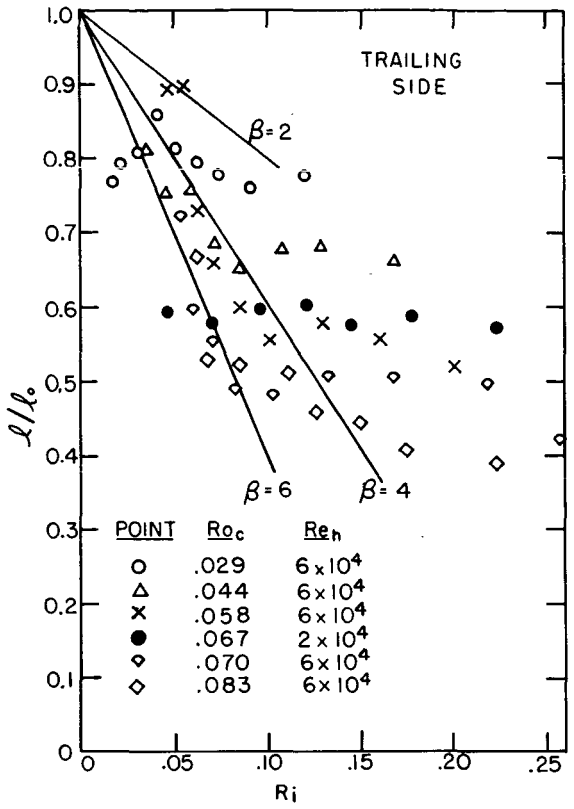

FIGURE 17.—*Mixing length ratio versus local gradient Richardson number on trailing side of channel; from data of reference 19.*

For small Ri, Bradshaw (ref. 7) suggests that a "Monin-Oboukhov" formula of the type

$$\frac{l}{l_0}=1-\beta Ri \tag{20}$$

might be useful to represent mixing length in flows with body force stabilization. This formula is plotted in figures 17 and 18 for values of $\beta=2$, 4 and 6. Values of β from 4 to 6 may be acceptable for very small Ri, but the uncertainty in the data is too high to draw a firm conclusion.

The Monin-Oboukhov type of formula was originally developed to represent l in density-stratified, atmospheric, turbulent shear flow for regions of approximately constant Ri. In nearly normal, turbulent boundary layers, Ri is not a constant and the use of this simple representation for most cases of practical interest will be, at best, a crude approximation.

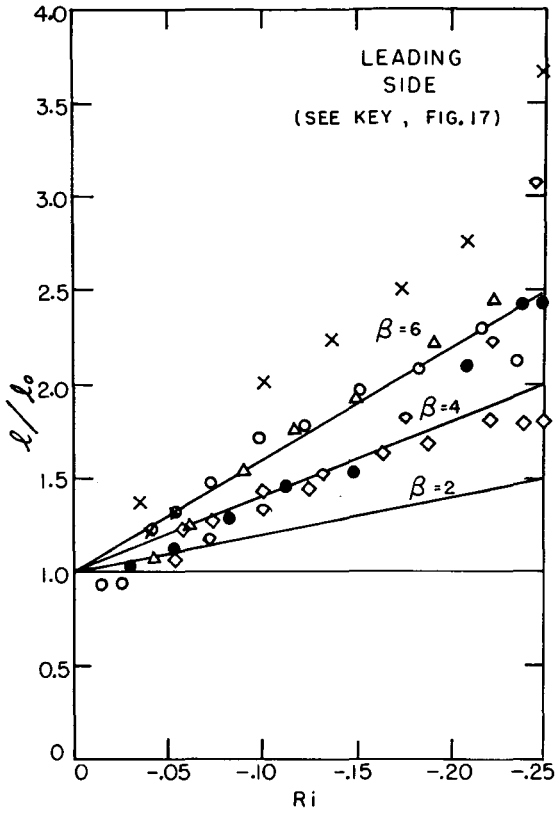

FIGURE 18.—*Mixing length ratio versus local gradient Richardson number on leading side of channel, from data of reference 19.*

Concluding Remarks

If the results of this section are to be employed in new boundary-layer computation methods, much remains to be done. To date, the ideas have only been used qualitatively in practice. For example, the two-dimensional, turbulent boundary-layer calculations shown by Litvai (ref. 32) for trailing side flow on a centrifugal impeller blade do not account for the effects of rotation on structure. His calculated results disagree with his measured results in a manner that tends to show that the experimental boundary layer remains transitional or laminar far downstream of the normal transition point. Qualitatively, this effect is to be expected from the results of this section. The influence of rotation on mixing in the shear layer above the trailing side wake region in Moore's recent experiments (ref. 37) on a rotating radial diffuser has already been quoted as a specific

qualitative example of the stabilizing influence of rotation on turbulence (see the section on radial passages, tubes, and ducts).

The successful inclusion of effects of rotation on turbulent structure in turbulent boundary-layer theory is most likely to be achieved in methods that attempt solution of the differential equations rather than momentum—or other—integral equation methods (see ref. 49) because of the greater ease of interpretation of the physical phenomena in the former methods. In the differential methods, direct use may be made of the equations for the components of Reynolds stress (e.g., table I) and/or simple equations such as the Monin-Oboukhov type of formula for mixing length may be employed.

ACKNOWLEDGMENT

The assistance of the author's past and present associates, in particular Mr. J. M. Kuhne, Dr. R. M. Halleen, and Mr. D. K. Lezius, is gratefully acknowledged.

LIST OF SYMBOLS

English Letters

AS	Aspect ratio, b/D
b	Half depth of duct between walls perpendicular to Ω
c_f	Skin friction coefficient, $\tau_w/(\rho/2)U^2$
D	Half width of duct between walls parallel to Ω
d	Diameter of round tube
d_h	Hydraulic diameter
e	Rate of viscous dissipation of turbulence energy, $\overline{q'^2}$ (see eq. (16))
f_i	Rectangular components ($i=1, 2, 3$) of Coriolis acceleration vector (see eq. (24))
$\hat{f}$	Friction factor for tube or duct flow
L	Characteristic spatial dimension
l	Mixing length, $\sqrt{\tau/\rho}/(d\bar{u}/d\eta)$
P_{ij}	Total rate of production of turbulent energy and/or stress
p	Static pressure
p^*	Reduced static pressure, $p-\omega^2r^2/2+\Phi$
q'^2	Instantaneous turbulence energy, $(u'^2+v'^2+w'^2)/2$
Re	Reynolds number, UL/ν
Re_δ	Boundary layer thickness Reynolds number, $U_\infty\delta/\nu$
Re_h	Tube or duct Reynolds number, $\bar{u}_m d_h/\nu$
Ri	Gradient Richardson number, $S(1+S)$
Ro	Rotation number, $2\omega L/U$

Ro_δ	Boundary layer rotation number, $2\Omega\delta/U_\infty$
Ro_c	Channel (rectangular duct) rotation number, $2\omega D/\bar{u}_m$
Ro_d	Round tube rotation number, $\omega d/\bar{u}_m$
Ros	Rossby number, $U/\omega L$
r	Radial distance from axis of rotation
r_{tip}	Impeller tip radius
S	Local mean profile parameter, $-2\Omega/(\partial\bar{u}/\partial y)$
U	Characteristic relative velocity
U_∞	Free-stream relative velocity
u, v, w	Components of relative velocity in x, y, z coordinate directions
u_i	Rectangular components of relative velocity $(i=1, 2, 3)$
$\bar{u}^+$	Wall shear normalized mean velocity, $\bar{u}/u_\tau$
u_τ	Wall shear velocity, $\sqrt{\tau_w/\rho}$
u_{tip}	Impeller tip speed
x, y, z	Rectangular Cartesian coordinates used where $\boldsymbol{\Omega}$ along z axis
x_i	Rectangular Cartesian coordinates $(i=1, 2, 3)$

Greek Letters

β	A parameter (see eq. (20))
δ	Boundary layer thickness
η	Distance normal to a wall
η^+	Law of the wall coordinate, $\eta u_\tau/\nu$
λ	Disturbance wave length
ν	Kinematic viscosity
$\bar{\xi}_{abs}$	Absolute mean vorticity for two-dimensional shear flow, $2\Omega-(\partial\bar{u}/\partial y)$
ρ	Fluid density
τ	Fluid shear stress, $\nu\rho(\partial\bar{u}/\partial y)+(-\rho\overline{u'v'})$, in two-dimensional shear flow
τ_w	Wall shear stress
Φ	Scalar potential for conservative body force
Ω	Coordinate rotation vector for case of $\boldsymbol{\Omega}$ along z axis
Ω_i	Rectangular components of $\boldsymbol{\Omega}$ $(i=1, 2, 3)$
ω	Coordinate rotational speed (magnitude)

Superscripts and Subscripts

$'$	Fluctuating component of a nonsteady quantity; i.e., $u=\bar{u}+u'$
$-$	Time mean value of a quantity
m	Mass average across flow of a quantity
0	Quantity evaluated at zero-rotation condition with all other conditions and parameters held fixed
T	Wall value of quantity on trailing (suction) side
L	Wall value of quantity on leading (pressure) side

APPENDIX I

Equations of Motion in Steadily Rotating Coordinates

The continuity equation and the dynamic equations of motion for a fluid in motion relative to observer coordinates rotating at a steady rate $\Omega_i (d\Omega_i/dt = 0)$ about an axis fixed in inertial space will be displayed and discussed briefly for the general case and the case of constant density and constant viscosity Newtonian fluids. Cartesian subscript notation, including the repeated dummy index convention to indicate summation, will be used. However, the general vector notation will be used, where convenient, to increase understanding. For example, the system rotation vector is $\Omega_i = \boldsymbol{\Omega}$, and the fluid velocity vector, relative to the rotating system, is denoted by $u_i = \mathbf{u}$.

The *continuity* equation in the rotating system is no different than in inertial coordinates,

$$\frac{\partial \rho}{\partial t} + \frac{\partial}{\partial x_j}(\rho u_j) = 0 \tag{21}$$

For constant density fluids, it is

$$\frac{\partial u_j}{\partial x_j} = 0 \qquad \text{or} \qquad \boldsymbol{\nabla} \cdot \mathbf{u} = 0 \tag{22}$$

The *dynamic equations* of motion contain two additional inertia terms, the Coriolis and centrifugal acceleration terms. The *Coriolis acceleration* vector is

$$\mathbf{f} = 2\boldsymbol{\Omega} \times \mathbf{u} \tag{23}$$

or, in Cartesian tensor notation,

$$\mathbf{f} = f_i = 2 e_{ijk} \Omega_j u_k \tag{24}$$

where e_{ijk} is the unit cyclic coefficient.[12] The *centrifugal acceleration* caused by system rotation is $\boldsymbol{\Omega} \times (\boldsymbol{\Omega} \times \mathbf{r}_0)$ where $\mathbf{r}_0$ is a position vector originating at a fixed point 0 on the axis of rotation. If r is defined as the radial distance from the axis to any coordinate point x_i in the rotating system, this term is expressed as

$$\boldsymbol{\Omega} \times (\boldsymbol{\Omega} \times \mathbf{r}_0) = -\omega^2 r \frac{\partial r}{\partial x_i} = -\frac{\partial (\omega^2 r^2/2)}{\partial x_i} \tag{25}$$

---

[12] $e_{ijk} = 0$ unless $i \neq j \neq k$; $e_{ijk} = 1$ if ijk in cyclic order (1231...); $e_{ijk} = -1$ if ijk in anticyclic order (3213...).

where ω is the constant magnitude of $\boldsymbol{\Omega}$. Using this equation, the dynamic *equations of motion* are

$$\frac{Du_i}{Dt}+f_i-\frac{\partial(\omega^2r^2/2)}{\partial x_i}=-\frac{1}{\rho}\frac{\partial p}{\partial x_i}+X_i+\frac{\partial\tilde{\sigma}_{ij}}{\partial x_j} \tag{26}$$

where

$$\frac{Du_i}{Dt}=\frac{\partial u_i}{\partial t}+u_j\frac{\partial u_i}{\partial x_j}$$

is the acceleration of a fluid particle relative to the rotating coordinate system; p is the fluid static pressure; X_i the sum of all externally imposed body forces; and $\tilde{\sigma}_{ij}$ is the deviatoric stress tensor. The left-hand side of equation (26) is the absolute acceleration of the particle with respect to inertial space.

It is noted that the centrifugal acceleration term is the gradient of a scalar potential, $-\omega^2r^2/2$. If all body forces are conservative, and if the fluid may be assumed of constant density, it is convenient to define a *reduced pressure*

$$p^*\triangleq p-\frac{\rho}{2}\omega^2r^2+\Phi \tag{27}$$

where Φ is the scalar potential of the body forces $X_i=-\partial\Phi/\partial x_i$. A single term, $\partial p^*/\partial x_i$, can then replace three terms in equation (26). Further, if we are dealing with a Newtonian fluid of constant kinematic viscosity, ν, equation (26) reduces to the rotational form of the *Navier-Stokes equations* for constant ρ and ν.

$$\frac{Du_i}{Dt}+f_i=-\frac{1}{\rho}\frac{\partial p^*}{\partial x_i}+\nu\frac{\partial^2u_i}{\partial x_j\partial x_j} \tag{28}$$

Euler's equations for constant density are obtained by setting $\nu=0$. The primary advantage of using these forms which utilize p^* rather than p is to show, for constant density flow, that the rotation-induced centrifugal term plays no essential role in determination of the u_i field in flows without free surfaces where boundary and initial conditions are specified in terms of conditions on u_i (no slip condition, etc.). Equations (22) and (28) form a complete set in the variables u_i and p^*.

APPENDIX II

Elementary Dimensional Analysis

All considerations in this section assume that ρ and ν are constant; hence equations (22) and (28) are used. Assume that L is the relevant scale size of the flow field, U the relative velocity scale, and ω the dimensional rotary speed of the observational coordinates. If each term in equations (22) and (28) is appropriately nondimensionalized in terms of L, U, and ω so that

$$\hat{u}_i = Uu_i \qquad \hat{p}^* = \rho U^2 p^*$$

$$\hat{x}_i = Lx_i \qquad \hat{t} = Lt/U$$

$$\hat{\Omega}_i = \omega\Omega_i$$

where hatted variables are dimensional, then equations (22) and (28) become, when normalized

$$\frac{\partial u_j}{\partial x_j} = 0 \tag{29}$$

and

$$\frac{\partial u_i}{\partial t} + u_j \frac{\partial u_i}{\partial x_j} + \frac{1}{Ros} e_{ijk}\Omega_j u_k = -\frac{\partial p^*}{\partial x_i} + \frac{1}{Re}\frac{\partial^2 u_i}{\partial x_j \partial x_j} \tag{30}$$

$Re = UL/\nu$ is the Reynolds number and $Ros = U/2\omega L$ is the Rossby number which expresses the ratio of inertial to Coriolis accelerations.

If $Ros \gg 1$, Coriolis effects should be small, but if $Ros \ll 1$, the inertial acceleration terms in equation (30) are generally neglected. If both $Ros \ll 1$ and $Re \gg 1$, the geostrophic approximation, pressure terms are said to just balance the Coriolis accelerations; i.e., Du_i/Dt and $\partial^2 u_i/(\partial x_j \partial x_j)$ may be neglected in equations (30) and (28).

Many other methods of normalization exist in the literature of rotating flows. The normalizing definitions, depending on how they are to be used, lead to various useful parameters and simplifications of the basic equations. For example, if equation (30) is multiplied by Ros, another parameter, $E = Ros/Re = \nu/2\omega L^2$, representing the ratio of viscous to Coriolis forces, appears. The inverse of the Ekmann number is a special form of the Taylor number, $Ta = E^{-1}$. Only in certain very special cases may rotating flows be characterized in terms of a single dimensionless parameter. The Ekmann boundary layer (ref. 12) is an example where E is the single controlling parameter, rather than E and Ros. In turbomachines, we have generally found Re and the Rotation number, $Ro = Ros^{-1}$, to be the most useful. For example, Ro is convenient in presentation of results, since $Ro \to 0$ as $\omega \to 0$ whereas $Ros \to \infty$, and the case of $Ro < 1.0$ (or small Ro) is the most common situation.

REFERENCES

1. Acosta, A. J., and R. D. Bowerman, An Experimental Study of Centrifugal Pump Impellers. *Trans. ASME*, Vol. 79, No. 8, 1957, pp. 1821–1839.
2. Banks, W. H. H., and G. E. Gadd, *A Preliminary Report on Boundary Layers on Screw Propellers and Simpler Rotating Bodies.* Aeronautical Research Council ARC 23,423, FM3150, 1962.
3. Barna, S. N., Secondary Flow in a Rotating Straight Pipe. *Proc. Roy. Soc. London*, Ser. A, Vol. 227, 1954, pp. 133–139.
4. Benton, G. S., The Effects of the Earth's Rotation on Laminar Flow in Pipes. *Trans. ASME, J. Appl. Mech.*, Vol. 23, 1956, pp. 123–127.
5. Benton, G. S., and D. Boyer. Flow Through a Rapidly Rotating Conduit of Arbitrary Cross-Section. *J. Fluid Mech.*, Vol. 26, Part 1, 1966, pp. 69–80.
6. Boyer, D. L., *Flow Through a Rapidly Rotating Rectangular Channel.* Ph.D. dissertation, Johns Hopkins U., 1965.
7. Bradshaw, P., The Analogy Between Streamline Curvature and Buoyancy in Turbulent Shear Flow. *J. Fluid Mech.*, Vol. 36, Part 1, 1969, pp. 177–191.
8. Cham, T., and M. R. Head, Turbulent Boundary Layer Flow on a Rotating Disc. *J. Fluid Mech.*, Vol. 37, Part 1, 1969, pp. 129–148.
9. Chandrasekhar, S., *Hydrodynamic and Hydromagnetic Stability.* Oxford U. Press, 1961, Chapter II and pp. 36–42.
10. Conrad, P. W., *The Effects of Rotation on the Stability of Laminar Layers on Curved Walls.* Report FLD 9, Mech. Eng. Dept., Princeton U., August 1962.
11. Dean, R. C., Jr., *On the Unresolved Fluid Dynamics of the Centrifugal Compressor.* Presented at ASME Gas Turbine Division Conference (Washington, D.C.), March 17–21, 1968.
12. Ekmann, V. W., On the Influence of the Earth's Rotation on Ocean Currents. *Arkiv Mat. Astr. Fys.*, Vol. 2, November 11, 1905.
13. Fischer, K., and D. Thoma, Investigation of Flow Conditions in a Centrifugal Pump. *Trans. ASME*, Vol. 54, pp. 141–155.
14. Fowler, H. S., *Some Measurements of the Flow Patterns in a Centrifugal Compressor Impeller.* ASME Paper 65-WA/GTP-7, 1965.
15. Fowler, H. S., The Distribution and Stability of Flow in a Rotating Channel. *Trans. ASME*, Ser. A., Vol. 90, July 1968, pp. 229–236.
16. Fujie, K., Three-Dimensional Investigation of Flow in Centrifugal Impeller With Straight-Radial Blades. *Bull. Japan Soc. Mech. Eng.*, Vol. 1, No. 1, 1958, pp. 42–49. See also Vol. 1, No. 3, 1958, pp. 275–282, and Vol. 4, No. 13, 1961, pp. 94–101.
17. Görtler, H., *On the Three-Dimensional Instability of Laminar Boundary Layers on Concave Walls.* Translated from original in NACA, TM 1375, June 1954.
18. Gregory, N., J. T. Stuart, and W. S. Walker, On the Stability of Three-Dimensional Boundary Layers With Application to the Flow Due to a Rotating Disc. *Phil. Trans. Proc. Roy. Soc. (London)*, A 248, 1955, p. 155.
19. Halleen, R. M., and J. P. Johnston, *The Influence of Rotation on Flow in a Long Rectangular Channel—An Experimental Study.* Report MD-18, Thermoscience Division, Dept. Mech. Eng., Stanford U., May 1967.
20. Hamrick, J. T., J. Mizisin, and D. J. Michel, *Study of Three-Dimensional Internal Flow Distribution Based on Measurements in a 48-Inch Radial-Inlet Centrifugal Impeller*, NACA TN 3101, February 1954.
21. Hill, P. G., and I. M. Moon, *Effects of Coriolis on the Turbulent Boundary Layer in Rotating Fluid Machines.* Gas Turbine Lab. Report 69, M.I.T., June 1962.
22. Himmelskamp, H., *Profiluntersuchungen an Einem Umlaufenden Propeller.* Mitt. Max-Planck-Inst. 2, 1950.

23. HORLOCK, J. H., Boundary Layer Problems in Axial Turbomachines. *Flow Research on Blading.* (Proc. Brown Boveri Symposium), L. S. Dzung, ed., Elsevier Press, 1970.
24. HOWARD, J. H. G., Analytical Theory of Secondary Flow in a Centrifugal Impeller. *Trans. Eng. Inst. Canada,* Vol. 9, No. B-1, Paper No. EIC-66-Mech 4, April 1966.
25. HOWARD, J. H. G., AND E. LENNEMANN, *Measured and Predicted Secondary Flows in a Centrifugal Impeller.* ASME Paper 70-GT-55, ASME Gas Turbine Conference, May 1970.
26. JOHNSTON, J. P., AND R. C. DEAN, JR., Losses in Vaneless Diffusers of Centrifugal Compressors and Pumps. *Trans. ASME,* Ser. D, Vol. 88, No. 1, 1964, pp. 49–62.
27. VON KÁRMÁN. T., Über Laminare und Turbulente Reibung. *Z. Angew. Math. Mech.,* Vol. 1, 1921, p. 233.
28. KAYE, J., AND E. C. ELGAR, Modes of Adiabatic and Diabatic Fluid Flow in an Annulus With an Inner Rotating Cylinder. *Trans. ASME,* Vol. 58, 1958, pp. 753–765.
29. KLINE, S. J., W. C. REYNOLDS, F. A. SCHRAUB, AND P. W. RUNSTADLER, The Structure of Turbulent Boundary Layers. *J. Fluid Mech.,* Vol. 30, Part 4, 1967, pp. 741–773.
30. KRAMER, J. J., AND J. D. STANITZ, *A Note on Secondary Flow in Rotating Radial Channels.* NACA Report 1179, 1954.
31. LAKSHMINARAYANA, B., *Investigations and Analysis of Flow Phenomena of Secondary Motions in Axial Flow Inducers.* Dept. Aerospace Eng., Penn State U., May 1968.
32. LITVAI, E., *Discussion in Flow Research on Blading.* L. S. Dzung, ed., Elsevier Press, 1970, p. 392.
33. LOHMANN, R. P., An Investigation of the Influence of the Boundary Layers on the Performance of Centrifugal-Compressor Impellers. *Trans. ASME,* Ser. D., Vol. 88, No. 1, 1966, pp. 71–81.
34. MELLOR, G., Laminar Flow and Transition. *Effect of Curvature and Rotation on Boundary Layer Development, Part I.* Ingersoll-Rand Co., Advanced Eng. Dept., TM66, February 1961.
35. MOON, I. M., *Effects of Coriolis Force on the Turbulent Boundary Layer in Rotating Fluid Machines.* Gas Turbine Lab Report 74, M.I.T., June 1964.
36. MOORE, J., *Effects of Coriolis on Turbulent Flow in Rotating Channels.* M.I.T., Gas Turbine Lab Report 89, January 1967.
37. MOORE, J., *The Development of Turbulent Layers in Centrifugal Machines.* M.I.T., Gas Turbine Lab Report 99, June 1969.
38. PATEL, V. C., *Measurements of a Secondary Flow in the Boundary Layers of a 180 Degree Channel.* ARC 30428, FM 3975, 1968; available as AD 679430 from Clearinghouse, DDC.
39. POTTER, M. C., AND M. D. CHAWLA, *The Stability of Boundary Layer Flow Subject to Rotation.* Private communication, 1970. See also M. D. Chawla, Ph.D. dissertation, Michigan State U., 1969.
40. RAYLEIGH, J. W. S., On the Dynamics of a Revolving Fluid. *Proc. Roy. Soc. (London).* Vol. 6A, 1916, pp. 148–154.
41. SENOO, Y., AND R. C. DEAN, JR., Rotating Wakes in Vaneless Diffusers. *Trans ASME,* Ser. D, Vol. 82, 1960, pp. 563–574.
42. SENOO, Y., M. YAMAGUCHI, AND M. NISHI, A Photographic Study of the Three-Dimensional Flow in a Radial Compressor. *Trans. ASME,* Ser. A, Vol. 90, No. 3, 1968, pp. 237–244.
43. SHIH-I, PAI, *Turbulent Flow Between Rotating Cylinders.* NACA, TN 892, 1939.

44. SMITH, A. G., On the Generation of the Streamwise Component of Vorticity for Flows in Rotating Passages. *Aeron. Quart.*, Vol. 8, November 1957, pp. 369–383.
45. TAYLOR, G. I., Stability of a Viscous Liquid Contained Between Two Rotating Cylinders. *Phil. Trans. Roy. Soc.* (*London*), Ser. A, Vol. 223, 1923, pp. 289–343.
46. TOWNSEND, A. A., *The Structure of Turbulent Shear Flow*. Cambridge U. Press, 1956, Chapter 2.
47. TREFETHEN, L., Fluid Flow in Radial Rotating Tubes. *Actes, IX^e Congrés International de Méchanique Appliquée*, Vol. II, Bruxelles U., 1957, pp. 341–350.
48. TREFETHEN, L., *Flow in Rotating Radial Ducts*. General Electric Engineering Laboratory, Report 55GL350-A, August 1957.
49. KLINE, S. J., G. SOVRAN, M. V. MORKOVIN, AND D. J. COCKRELL, eds., *Proc., Computation of Turbulent Boundary Layers-1968 AFOSR-IFP-Stanford Conference*. Thermosciences Div., Dept. of Mech. Eng., Stanford U.
50. LEZIUS, D. K., AND J. P. JOHNSTON, *The Structure and Stability of Turbulent Wall Layers in Rotating Channel Flow*, Rept. MD-29, Thermosciences Div., Dept. Mech. Eng., Stanford U., 1971.

DISCUSSION

J. GRUBER (Technical University of Budapest): First of all, I should like to congratulate the author on his excellent paper dealing with some extremely important problems in the field of turbomachinery. His statements concerning the Coriolis forces which influence the stability of the boundary layer seem especially valuable. According to his statements, the rotation modifies the law of the wall. The experiments carried out in the Laboratory of Fluid Mechanics of the Technical University of Budapest support these findings (refs. D–1, D–2, and D–3). The developing turbulent boundary layer on the blading of a centrifugal impeller has been studied, and the research has been extended to the law of the wake too.

In my opinion, the feasibility of accurately measuring the wall shear stress will have a definite importance in further research, and therefore I have two questions in connection with the author's paper:

(1) Does the author intend to repeat the wall shear stress measurements with the Ludwieg method, applying a flush-mounted, quartz-coated, heated film probe, in addition to the Preston tube method?

(2) Did the author consider extending the law of the wall for a stationary flow to a rotating case as follows?

$$\bar{u}^+ = \frac{u}{u_\tau} = F\left[\left(\frac{\eta u_\tau}{\nu}\right), \left(\frac{\Omega \eta}{u_\tau}\right)\right]$$

(The designations are the same as those of the author.)

P. G. HILL (Queen's University): The writer would like to express appreciation for the comprehensive and valuable review Dr. Johnston has given of Coriolis effects in channel flows.

The effects of rotation on channel flow are difficult to discern and categorize, not only because of instrumentation problems, but especially because of the problems of designing a controlled experiment. In general, the boundary conditions (e.g., relative rotationality of the inlet flow) are naturally affected by rotation, so that as the rotational speed of the experimental channel is changed, the problem itself is altered. The effect of rotation on separation, for instance, could be as strongly dependent on change of inlet boundary condition as on either the secondary flow or the stabilizing/destabilizing mechanism. Such effects could of course be understood by the results of inviscid flow calculations if they occurred in

isolation. However, in channels of low aspect ratio with thick boundary layers, there is generally a strong interaction between these mechanisms.

Adding somewhat to the general problem of sorting out what is going on is the difficulty of deciding when secondary flow may be neglected. In constant-area channels at high aspect ratio (e.g., 7:1) it appears, as Dr. Johnston has noted, that secondary flow is negligible at the midplane for quite large values of the rotation parameter. However, for diffusing flows, even at high aspect ratio, this is probably far from realistic. At aspect ratios typical of centrifugal machine impellers (i.e., of order unity) there seems little doubt that secondary flows are very important, if not dominant.

The significance of the work of Moore (ref. 37) in this connection appears to be in demonstrating that (albeit with a very approximate model) stationary flat-plate, three-dimensional boundary-layer techniques can provide a physically realistic description of the flow without direct inclusion of the effects of Coriolis force on turbulence quantities. Although this result suggests that secondary-flow effects are dominant, it does not rule out the possibility that the effect of Coriolis force on turbulence may have a significant effect on separation and mixing losses in impellers. The effect of Coriolis force on turbulence production has been shown in a most interesting way in the film by Johnston and Halleen and commented on in this paper with respect to the turbulent energy equation. It would be of great interest if the author would give his views on the need for, and possible means of, incorporating these effects into turbulent boundary-layer calculation procedures.

A. S. MUJUMDAR (Carrier Corporation): Litvai and Preszler (ref. D–3) have recently published some data on the velocity profile of the turbulent boundary layer on rotating impeller bladings which indicate that the law of the wall holds in the case of a rotating system as well. Using the conventional notation, the law of the wall may be expressed as

$$u^+ = A \log y^+ + B \tag{D–1}$$

The constants A and B were correlated in terms of a rotation parameter, Ω, defined by

$$\Omega = 2\omega(u^+)^2 \tag{D–2}$$

where ω is the rotational speed. The major effect of rotation was assumed to be confined to A.

The effect of rotation on the slope in the universal velocity distribution was determined by considering the turbulent boundary-layer flow as a damped, forced vibrating system. The stabilizing (damping) effect of the Coriolis forces was regarded as essentially a change in the spring constant of the system. After a series of approximations, the authors derived the

following formula for the slope of the logarithmic velocity profile:

$$A = A_0(1+a\Omega)^{1/2} \qquad \text{(D–3)}$$

where A_0 is the slope in the absence of rotation and a is a constant which may be determined experimentally. In spite of rather large scatter in the data, equation (D–3) indicates the correct trend; i.e. for $\Omega > 0$, which corresponds to the suction side of the blade, the slope of the velocity profile is steeper. The converse is also true.

It may be noted that the data are limited to very low rotational speeds, the maximum shaft speed being only 18 rpm.

J. MOORE (General Electric Co.): Dr. Johnston has given a stimulating description of the studies of simplified flows which sheds some light on the flows in turbomachine rotors. It is, however, sobering to read Dean's description (ref. 11) of the real situation in centrifugal impellers and compare the unknowns with the mostly qualitative explanations.

Dean has provided several observations of rotational effects for quantitative explanation and prediction.

(1) A relatively quiescent wake on the suction (trailing) side of an impeller passage, which may contain as much as 20 percent of the through flow.

(2) The relative absence of turbulent mixing between the wake and the rest of the flow, which flows as a "jet" along the pressure side.

(3) The violent turbulence generated on the pressure surface of the blades above design incidence.

(4) Blades operating at $-25°$ incidence without any steady pressure side stalling.

These observations, as well as Dean's overall description of separation within the passage, provide challenges for the boundary-layer predictor.

Moore (ref. 37) has made a start towards predicting the occurrence and development of the "wake" and has shown that three-dimensional, integral boundary-layer techniques can give a quantitative description of the secondary-flow effects on all the boundary layers. It may well be, however, that "separation" within an impeller passage is not always governed by secondary flows, and it certainly seems to be often three-dimensional. But one can say that, if the flow in an impeller ever knows about the Taylor-Proudman theorem, it does so near the wall in the wake on the suction side.

The quantitative description of Coriolis stability effects by Bradshaw (ref. 7) is an encouraging start towards the solution of the differential equations. However, as Bradshaw points out, the linear Monin-Oboukhov formula applies only for the inner layer of the boundary layer which ends at $u_\tau y/\nu = 200$. Certainly the absence of turbulent mixing between the jet and wake occurs in the outer layer, and Dean's pressure side observations

may also be outer-layer phenomena. It seems that the Coriolis stability effects in the outer layer (in particular the "wake") should receive more experimental attention.

One hopes that more studies of simplified flows will be undertaken to shed light on these still dimly lit phenomena.

JOHNSTON (author): Of the various points raised in discussion at least two require some additional comment. Both of the following remarks relate to the effects of Coriolis stabilization on two-dimensional turbulent boundary layers. The first, prompted by Professor Gruber's and Mr. Mujumdar's discussions, concerns the law of the wall for the inner, fully turbulent parts of the layer, whereas the second is made in connection with Dr. Moore's comments on the outer layer and the turbulent free-shear layers that occur on the edge of separated regions.

Dimensional analysis gives the general form of the law of the wall. Professor Gruber presents it in the form

$$\bar{u}^+ = F(\eta^+, \Omega^+\eta^+) \tag{D-4}$$

Ω^+ is the wall-layer rotation parameter ($\Omega^+ = \Omega\nu/u_\tau^2$) and η^+ is the dimensionless distance from the wall ($\eta^+ = \eta u_\tau/\nu$). Ω, and hence Ω^+, is negative for trailing (suction) surface layers and positive for leading (pressure) side layers. The data of Gruber, Litvai and Preszler (refs. D–1, D–2, and D–3) and that of Halleen and Johnston (ref. 19) suggest that $\bar{u}^+$ is higher than its zero-rotation value for given η^+ when Ω^+ is negative (suction side) and vice versa for positive Ω^+ (pressure side) conditions; see figure 13, for example.

The wall layer parameter Ω^+ may be related to the stability parameters S and Ri by application of basic definitions, e.g.

$$S = -\frac{2\Omega}{\partial\bar{u}/\partial\eta} = -\frac{2\Omega l}{\sqrt{\tau/\rho}} \tag{D-5}$$

If it is assumed, as is commonly done in the wall layer region, that fluid shear stress τ equals the wall shear stress, $\tau_w = \rho u_\tau^2$, equation (D–5) becomes

$$S = -2\Omega^+ \frac{lu_\tau}{\nu} \tag{D-6}$$

Furthermore, in the turbulent part of the wall-layer region the zero-rotation mixing length l_0 is approximately $\kappa\eta$ where $\kappa \approx 0.4$ is the Karman constant. Thus equation (D–6) reduces to

$$S = -2\kappa\Omega^+\eta^+ \frac{l}{l_0} \tag{D-7}$$

By assuming that a relation such as the "Monin-Oboukhov" formula (eq. (20)) holds for the turbulent law of the wall regions, it is now seen from equations (D–7) and (2) that $\Omega^+\eta^+$ is directly related to S or Ri and at least two empirical constants K and β. This relationship can be expressed in the explicit form

$$Ri = S = -2\kappa\Omega^+\eta^+ \tag{D–8}$$

for the limiting conditions of very small rotation effects; i.e., when $Ri \approx S$ and $l/l_0 \approx 1$ or, alternatively, when $[\Omega^+] \ll 1$. Note that this limiting case is independent of β, whose value is not yet well established.

Two specific forms for the turbulent region law of the wall have been proposed for rotationally stabilized flows: that of Bradshaw (ref. 7) and that of Litvai and Preszler (ref. D–3).

Bradshaw used the "Monin-Oboukhov" formula and the assumptions $\tau = \tau_w$ and $Ri = S$ (small rotation effects) to obtain the formula

$$\bar{u}^+ = \frac{1}{\kappa} \ln \eta^+ + B - 2\beta\Omega^+\eta^+ \tag{D–9}$$

He found that this form fit Halleen's data quite well for $\eta^+ \lesssim 500$ with a value of $\beta \approx 4$ for $S > 0$ (stable conditions) and $\beta \approx 2$ for $S < 0$ (unstable conditions). The values of Ω^+ were small, in the range from 0.003 to 0.012, for all the data he used (that shown in fig. 13) in checking equation (D–9).

The formulation by Litvai and Preszler (ref. D–3) is presented by Mujumdar in his discussion. It may be recast in the form

$$\bar{u}^+ = \frac{1}{\kappa} (1 + \gamma S)^{1/2} \ln \eta^+ + B \tag{D–10}$$

if one notes that α, the turbulence frequency used in reference D–3, may be expressed as $\gamma\alpha = \partial\bar{u}/\partial\eta$. γ is a dimensionless factor of proportionality that allows α to equal $\partial\bar{u}/\partial\eta$, the local scale of turbulence frequency in a shear layer. γ should be of unity order of magnitude and, as we shall try to show, should be closely related to the factor β of equation (20). The formula shown above seems much more satisfactory than the original as *all* parameters and variables are now dimensionless and S, the stability parameter, appears explicitly.

The formulas given in equations (D–9) and (D–10) may be directly compared for the case of small rotation effects if the term $(1+\gamma S)^{1/2}$ in equation (D–10) is expanded in a binomial series and terms of order $(\gamma S)^2$ and smaller are neglected. When equation (D–8) is used to replace S in the expanded result, equation (D–10) becomes

$$\bar{u}^+ = \frac{1}{\kappa} \ln \eta^+ + B - \gamma\Omega^+\eta^+ \ln \eta^+ \tag{D–11}$$

Since the rotation terms in equations (D–9) and (D–11) are small, the resulting fit of available data to either expression would be equally good if γ were taken to be a constant. The ratio $2\beta/\gamma = \ln \eta^+$ is not too far from constant (3.9 to 5.3) over the range of η^+ values (50 to 200) where data are normally expected to fit a turbulent law of the wall. Furthermore, for the range of probable β values (2 to 4, according to Bradshaw), γ is seen to be close to unity in value. Finally, there are still too few accurate velocity profile data to attempt to formulate more accurate law of the wall equations than those reviewed here. In fact, the need for a better formulation is not yet established.

I should like now to discuss briefly some new, preliminary observations that bear directly on the questions raised by Moore concerning the importance of Coriolis stabilization on the outer layers of turbulent boundary layers, and on free-shear layers in particular. In either case the magnitudes of the Richardson numbers can become quite large as $\partial\bar{u}/\partial\eta$ becomes small near the edge (or edges) of a shear layer. In particular, the value of Ri may be very large and positive in the free-shear layer separating the trailing side wake from the through-flow jet in separated centrifugal impeller flow (see Dean, ref. 11). The high degree of stability implied by such large positive Richardson numbers might indeed completely suppress turbulent transition in the wake-jet shear layer.

We have recently tried to examine the stability of the mixing layer formed over the separated flow that forms behind a backward facing step placed in our rotating channel apparatus. The low-speed ($\sim$1 ft/sec) water flow was observed using the hydrogen bubble technique with the generating wire placed in the free-shear layer and close to the step.

With positive Ω and thus negative (destabilizing) Richardson numbers, the mixing process was turbulent in the layer and qualitatively the same as at zero rotation; that is, two-dimensional, Kelvin-Helmholtz waves formed right behind the step and rapidly degenerated into fully three-dimensional turbulence a short distance downstream of the step. However, at the same unit Reynolds number, with the direction of rotation reversed so that Ω became negative and the Richardson number positive (stabilization) there was clear visual evidence that breakdown of the two-dimensional Kelvin-Helmholtz waves was severely retarded. At high negative rotational speeds, no ordinary turbulence was noted within the observable region of the shear layer that extended 3 to 4 inches downstream of the step.

In conclusion, our new observations tend to confirm those of Dean (ref. 11) and Moore (ref. 37) and lend credence to the idea of a quiescent wake mixing layer in separated centrifugal impeller flows. The full implications of these very preliminary investigations are yet to be appreciated. There certainly must, in addition, be important outer layer effects of rotation on unseparated turbulent boundary layers as pointed out by

Moore in his discussion. Much more research will be required to untangle these phenomena.

Finally, I wish to thank all the discussors for their generous and interesting comments and I am sorry that space does not permit comment on all points raised in discussion.

REFERENCES

D–1. GRUBER, J., AND E. LITVAI, An Investigation of the Effects Caused by Fluid Friction in Radial Impellers. *Proc. III Conf. on Fluid Mech. and Fluid Machinery*. Akadémiai Kiadó (Budapest), 1969, p. 241.

D–2. LITVAI, E., AND L. PRESZLER, The Velocity Profile of a Turbulent Boundary Layer on the Blading of Radial Impellers. *Proc. III Conf. on Fluid Mech. and Fluid Machinery*, Akadémiai Kiadó (Budapest), 1969, p. 348.

D–3. LITVAI, E., AND L. PRESZLER, On the Velocity Profile of the Turbulent Boundary Layer on Rotating Impeller Bladings. *Periodica Polytechnica, Mech. Eng.* (Budapest), Vol. 13, 1969, p. 215.